ANNALS OF GEOPHYSICS, 68, 1, V104, 2025; doi:10.4401/g-9157
OPEN ACCESS

An improved methodology for lava flow hazard mapping at Etna volcano

Cappello Annalisa*,[1], Giuseppe Bilotta[1], Francesco Zuccarello[1], Cristina Proietti[1], Gaetana Ganci[1]

(1) Istituto Nazionale di Geofisica e Vulcanologia, Osservatorio Etneo, Catania, Italy

Article history: received September 16, 2024; accepted January 23, 2025

Abstract

Lava flow hazard is a significant geological threat associated with volcanic activity. Understanding and quantifying this hazard is crucial for protecting communities, infrastructure, and the environment, especially in active volcanic areas like Etna. Here we propose a new probabilistic methodology for assessing the lava flow hazard at Etna volcano based on a 4,000 years-long dataset of eruptions and accurate statistical analyses. The methodology combines the probability of future vent opening, the probabilities of occurrence of individual classes of eruptions, and the weighted combination of lava flow simulations. These simulations are based on representative scenarios for each eruption class. The results are two maps, one for flank and one for summit eruptions, which provide the likelihood that a specific area will be affected by lava flow inundation during specific time intervals. Moreover, we present the first attempt to assess the hazard from both kinds of eruptions (flank and summit) that occur at Etna volcano. These hazard maps represent a fundamental support for local authorities, facilitating land-use planning, emergency management, and decision-making during eruptive crises at Etna volcano.

Keywords: GPUFLOW; Statistical analysis; Flank eruptions; Summit activity; Lava inundation

1. Introduction

Active volcanoes are a source of natural hazards with potentially catastrophic consequences on the political, social and economic welfare of populations under threat. Etna (Sicily, Italy; Fig. 1) is the largest active volcano in Europe, well-known for its persistent activity from the summit craters and frequent lateral eruptions forming from vents situated on its flanks (Branca and Del Carlo, 2005). Persistent summit activity does not represent a significant threat to the population areas, although important tourist facilities and infrastructures close to the central craters may be threatened, and accidents may affect people (especially tourists) close to the area interested by the volcanic phenomena (e.g. 16 March 2017; Cioni et al., 2023). Conversely, flank eruptions pose a serious danger to the towns located around the volcano, especially when the eruptive vents open at very low altitudes (Del Negro et al., 2019; Centorrino et al., 2021).

Over the last four centuries, the most destructive flank eruption occurred in 1669 when ~1 km^3 of lava erupted in about four months, producing a ~17.5 km long tube-fed lava flow field that partially destroyed the city of

Catania (Branca et al., 2013). In the last century, the town of Mascali was destroyed by lava flows in 1928, and the villages of Fornazzo and Randazzo were respectively threatened in 1979 and 1981 (Coltelli et al., 2012; Branca et al., 2017). Due to the potential social and economic disasters posed by flank eruptions at Etna, knowing the probability of a particular site being overrun by a lava flow can be useful during eruptive emergencies to plan crisis response activities and to recognize communities and infrastructure at risk (Mangiameli et al., 2025).

The hazard related to Etnean flank eruptions has been of scientific interest for decades. The first maps proposed hazard zonations mostly based on qualitative analysis of historical eruptions (e.g., Frazzetta and Romano, 1978; Guest and Murray, 1979; Duncan et al., 1981; Behncke et al., 2005), while the most recent ones are based on simulations

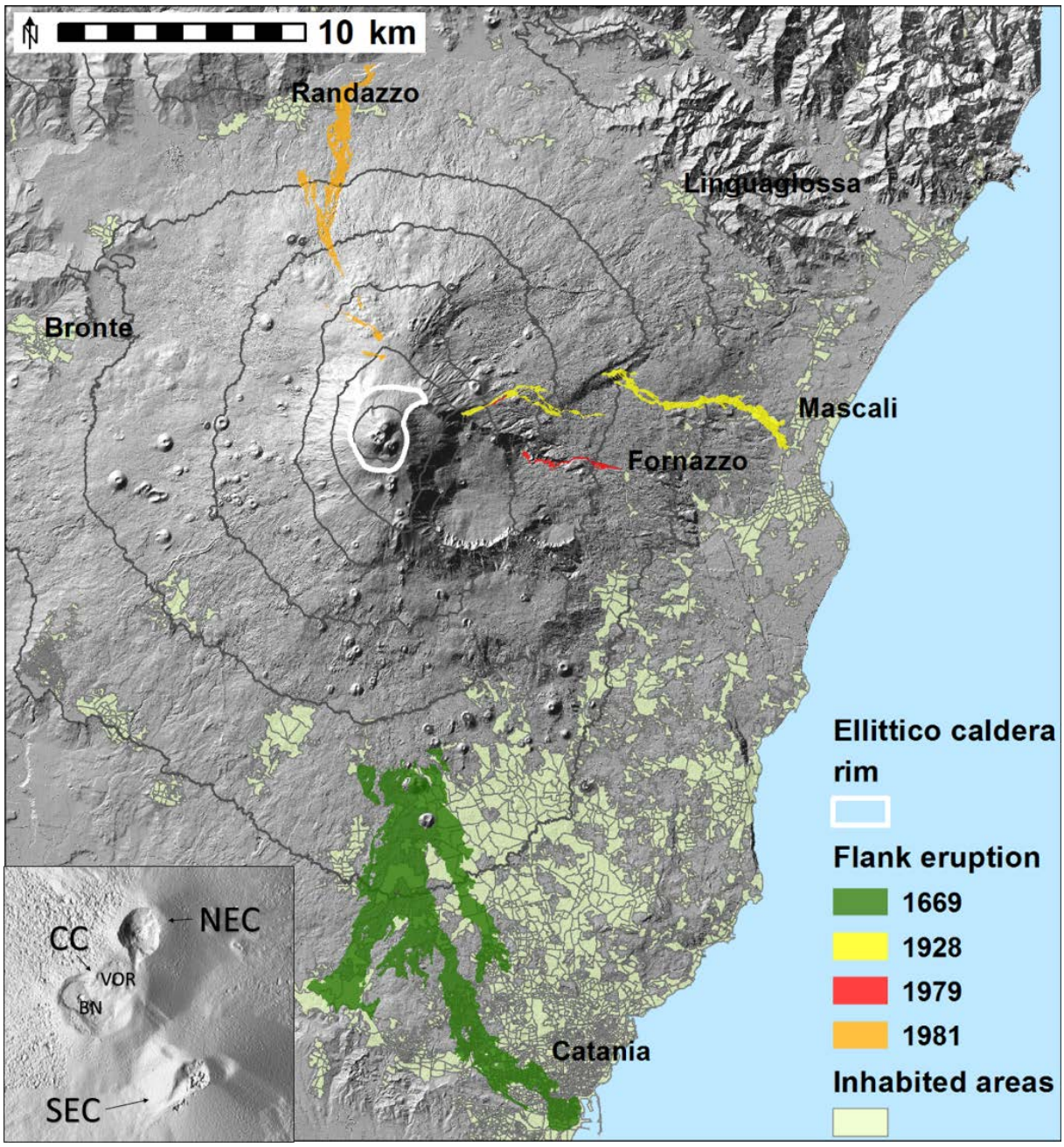

Figure 1. Etna's flank eruptions that destroyed or threatened towns and villages over the last 400 years. The background image is the shaded relief extracted from the 2005 Digital Surface Model (DSM) of Etna (Gwinner et al., 2005). Contour lines are from 3,000 to 0 meters a.s.l. (every 500 meters). The inset shows Etna's summit with the names of the main active craters: SEC (South-East Crater), NEC (North-East Crater), and CC (Central Crater), which includes BN (Bocca Nuova) and VOR (Voragine). The background image is the shaded relief of a satellite-derived DSM updated to July 2021 (Ganci et al., 2023).

performed by numerical models of different types and complexity (e.g., Wadge et al., 1994; Favalli et al., 2009; Crisci et al., 2010; Cappello et al., 2011a; 2011b; Del Negro et al., 2013b).

On the other hand, the hazard posed by lava flows from summit eruptions at Etna has been investigated in more recent times. This was especially due to the increasing activity of the South-East Crater (SEC) since 2011 (Cappello et al., 2019), the most active among the summit craters (North-East Crater: NEC; Central Crater: CC, which includes Bocca Nuova and Voragine; Fig. 1). This has led to the production of lava flow hazard maps for the SEC (Vicari et al., 2011; Cappello et al., 2019) and, in 2013, to the first hazard map for the summit area (Del Negro et al., 2013b). However, the notable morphological changes that Etna's summit area has undergone, due to both the emplacement of eruptive deposits and the partial collapses of the cones, make it necessary to continuously update these maps in order to always have accurate and up-to-date estimates.

Here we propose an updated estimate of the flank and summit lava flow hazard at Etna volcano based on a probabilistic approach that analyzes the lava flows of the last 4,000 years and the last century, respectively, and simulates possible lava flow paths using the new GPUFLOW model (Cappello et al., 2022). The two maps show the areas more likely to be inundated by lava flows during the next 30 years for flank eruptions, and 3 years for the summit activity. The shorter time projection for the summit eruptions is motivated by the current fast topographic evolution of the summit area. A unified hazard map was also developed by combining both types of eruptive activity, considering an exposure time of 10 years. The presented maps could be fundamental tools, especially in the long term, for emergency preparedness and territorial planning, allowing to easily identify the zones where future eruptions could have a higher impact. Moreover, they could help local authorities to deal with ongoing eruptions, make focused decisions, and mitigate the associated risks.

2. Lava flow hazard assessment

Our methodology to build the hazard map is developed in different stages, each one producing a specific product: the spatiotemporal probability map of future vent opening, the occurrence probabilities associated with classes of expected eruptions, a large number of eruptive scenarios simulated with the GPUFLOW model, and the effective long-term hazard map computed by merging the products obtained during the previous stages.

A detailed description of each stage is reported in the following sections.

2.1 Quantification of the vent opening probability

The first and maybe most important step in forecasting lava flow hazards involves the construction of a spatiotemporal probability map for the identification of the most probable emission zones of future lava flows, based on the analysis of the spatial location of past eruptive vents, as well as the eruption frequency within a time window (Selva et al., 2012; Cappello et al., 2015; Bevilacqua et al., 2017).

For flank eruptions, we reconstructed the most complete and up-to-date catalogue of flank fissures at Etna that opened in the last 4,000 years starting from the most recent and complete geological map of Etna (Branca et al., 2011; Proietti and Branca, 2024). Based on our statistical analysis, we produced the spatial vent opening map for flank eruptions using an Exponential kernel with a smoothing factor of 1,250 m (obtained by optimizing the fit between the training and testing datasets, see Sandri et al., 2024 for details), which shows that high-altitude flank fissures are two-to-three orders of magnitude more likely to occur than the low-altitude ones. It also confirms a North-East to South-East pattern of higher probability that involves the highest urbanized flank immediately upstream from the city of Catania (see Fig. 5 in Sandri et al., 2024). This map was rescaled considering a constant temporal rate of 0.988, estimated for the next 30 years by using a time-dependent model (Garcia-Aristizabal et al., 2012) on the flank eruptions that occurred since 1600.

For the summit eruptions, we separately considered eruptions of short and long durations that occurred in the last 40 years. Indeed, during paroxysmal activity, lava overflows lasting a few hours occur mostly from the main vents or from minor vents on the upper flanks of the summit cones. Long-lasting eruptions may also occur from sub-terminal fractures at hundreds of meters from the main vents. The spatial map for the long-lasting eruptions was obtained by using a 2D Gaussian kernel with a smoothing factor of 324 m (Zuccarello et al., 2023), showing that the highest probability is located southeast of SEC. The probability has been rescaled considering the temporal rate in a time

span of 3 years derived by using the power intensity function (Smerthurst et al., 2009). For the short-lasting eruptions, we considered the area surrounding the craters from the rims to 150-300 m, by distributing the temporal probability using a Gaussian kernel. The temporal probability has been estimated for each summit crater using a Discrete-Time Markov Chain approach, where 4 daily states were identified to build the transition matrix and calculate the probability of the lava fountaining state for the next three years (Zuccarello et al., 2023).

2.2 Characterization of the expected eruptions

2.2.1 Flank eruptions

Historical catalogues of Etna's flank eruptions starting from 1600 have been revised to define intervals of duration and volumes. The analysis of the trend of effusive rates of the most recent ones has led to the definition of generalized effusive rate curves to be used for both long- and short-term applications and the definition of classes of eruptions to be used for simulations (Zuccarello et al., 2022).

In total, we analyzed 63 flank eruptions (from 1610 to 2018) that occurred below 2,900 m a.s.l., for which sufficiently complete information on vent location, duration, and lava volume was available (Del Negro et al., 2013a; Proietti and Branca, 2024). To determine the eruption classes, we looked for a law correlating duration and volume, in order to estimate the distribution of the events within the appropriate error bands, and determine both "regular" events (where volume and duration would correlate) and "outliers" (for which volume and duration would not follow the law), as detailed blow.

A preliminary analysis was conducted on the duration of the flank eruptions, lasting from a minimum of 1 day to a maximum of 10 years, with a mean of 172 days and a standard deviation of 489 days, and quartiles at 8, 24 and 125 days. The set of eruptions was then split into "short" (lasting 7 days or less), and "long" (duration longer than a week) eruptions (Fig. 2a). This was done for two reasons: the first is the consideration that shorter events are more sensitive in the estimation of the coefficients of the law, and would thus produce noisier results; the second is led by the assumption that short events with a "regular" behavior would emit small amounts of lava and thus have limited influence in the hazard assessment, while short events with large mass fluxes would be outliers and would thus be better studied as a separate category.

For the "long" eruptions (48 events), a law in the form $V = k * \Delta T^n$ was used to fit the volume V against the duration ΔT. To find the optimal value of the exponent, we minimized the coefficient of variation of $V/\Delta T^n$ for n in the range [0, 1], obtaining $n = 0.500254$, which we approximate as $n = 0.5$, suggesting that the volume of an eruption is generally proportional to the square root of the duration. A statistical analysis of $V/\Delta T^{0.5}$ for the considered eruption allowed us to derive uncertainty bands for the proportionality coefficient k (Fig. 2b).

Nine eruptive classes were then identified, separated by the 25^{th} and 75^{th} percentile in duration (17 days and 173 days, respectively) and volume coefficient ($k = 2.88$ and $k = 9.28$, respectively). For each of these classes, a representative value was selected by picking a property (duration, volume coefficient) in the following way: if the class fits within the first quartile for said property, the 5^{th} percentile was taken as representative; if the class fit between the first and third quartile, then the median was taken as representative; and finally, for the classes beyond the third quartile, the 95^{th} percentile was taken as representative. The corresponding durations, coefficient k, and volumes for the nine classes are summarized in Table 1.

The effusion rate curve used for all classes has the same bell-shaped trend, which has been shown to reproduce well the general behavior of lava effusion rates related to the flank eruptions of Etna (Zuccarello et al., 2022). In particular, the effusion rates grow from 0 at the beginning of the eruption to a maximum at 1/4 of the total duration, then falling to an inflection point at 2/3 of the total duration, and then finally to 0 at the end. The mass flux at the inflection point is set as 1/3 of the peak mass flux (Fig. 3).

The remaining "short" eruptions were neglected for the calculation of the above law. However, a separate outlier class was considered to include those eruptions that have shown particular short duration and large volumes. This class has a total duration of 10 days, a peak of activity at 7 hours with 269 m^3/s and the inflection point of 72.7 m^3/sec after 42 hours. The data for this outlier class was taken from the 1928 and 1981 eruptions, which are considered among the most hazardous events of the last century at Mt. Etna (Zuccarello et al., 2022).

In summary, we obtained 10 eruptive classes (9 for the long-lasting ones plus 1 for the outliers), for which we estimated the probability of occurrence as the ratio between the number of eruptions belonging to that class and the total number of eruptions.

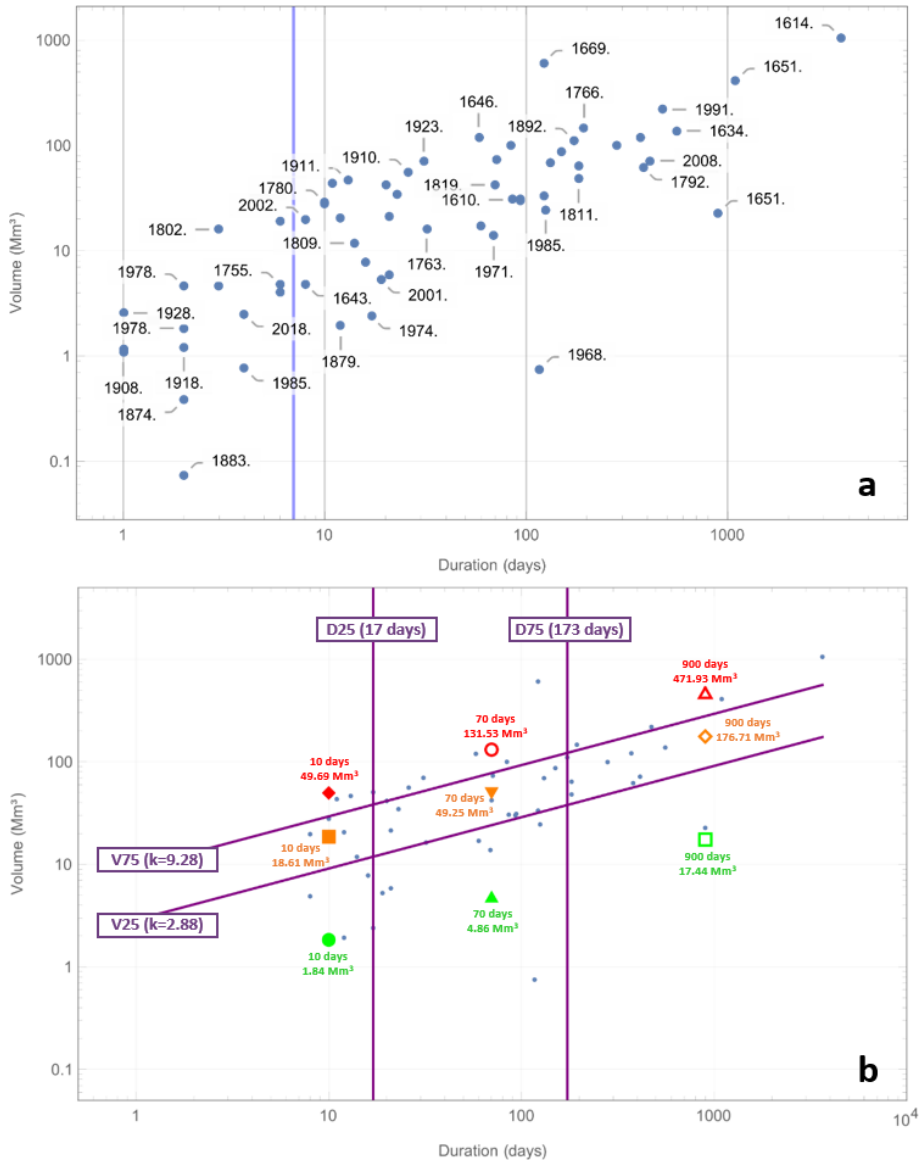

Figure 2. (a) Distribution of durations and lava volumes of the 63 flank eruptions that occurred at Etna since 1600 (some labels with the year of the eruption are superimposed on others and therefore not visible). The vertical blue line separates the "short" (less than a week) from the "long" (longer than a week) eruptions. (b) Distribution of durations and lava volumes of the 48 long eruptions. The violet lines represent the 25th and 75th percentiles, denoting the class separators. The representatives for each of the 9 classes (reported in Table 1) are also shown.

Duration percentile/ duration (d)	Volume percentile (k coefficient)		
	V05 (k = 0.58)	V50 (k = 5.88)	V95 (k = 15.7)
D05/10	1.84	18.61	49.69
D50/70	4.86	49.25	131.53
D95/900	17.44	176.71	471.93

Table 1. Duration and volumes for the 9 eruptive classes extracted from the "long" eruptions. Note that, while the duration for classes in the same row is the same, classes in the same column do not have the same volume, but the same coefficient *k* (represented here with two digits of precision). Lava volumes are in million cubic meters.

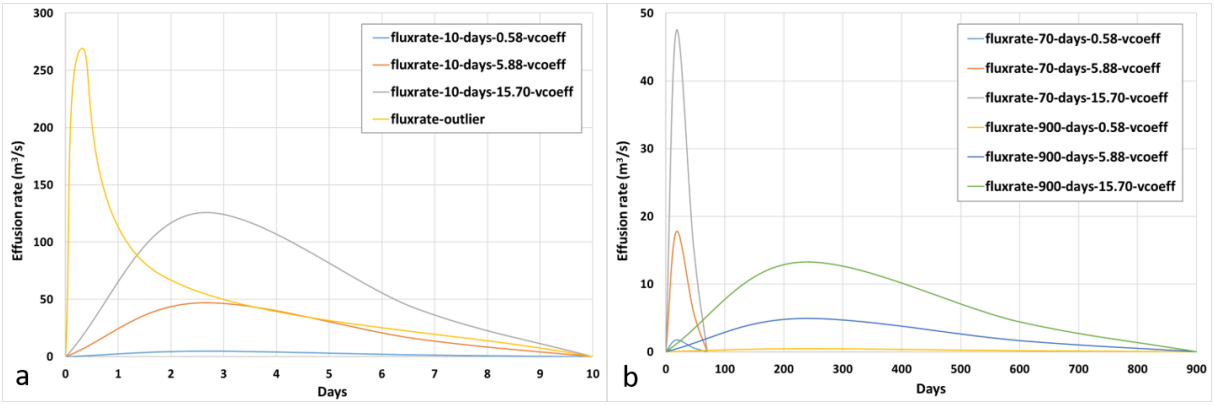

Figure 3. Effusion rate curves used for lava flow simulations characterizing flank eruptions (10 classes in total) with different volumes and durations at 10 (a), 70 and 900 days (b).

2.2.2 Summit eruptions

We also reviewed Etna's eruptions in the summit area, differentiating those emitted by NEC, CC, and SEC from the so-called sub-terminals, i.e. those produced by effusive vents located at the base of the summit craters within the area delimited by the rims of the Ellittico caldera (Fig. 1). This led to the discovery of two types of correlation between duration and total volume of lava, one for summit eruptions and one for sub-terminals, which allowed us to define characteristic classes of the two eruptive typologies (for details, see Zuccarello et al., 2023). In particular, short-lived summit eruptions, represented by lava fountains, constitute the 90th percentile of the distribution. For them, we defined three types of eruptive classes, with durations of 2-10 hours, volumes of 0.7-1.7 × 10^6 m^3, and a trapezoidal trend for the effusive rate defining its values during the pre-, syn- and post-fountain phases (Fig. 4a). For sub-terminal eruptions, three other classes have been defined. The respective effusion rate curves have been obtained by analyzing the temporal trends observed for events that occurred since 2006, with durations from 4 to 46 days and volumes of 1.5 – 7.9 × 10^6 m^3 (Fig. 4b).

Figure 4. Effusion rate curves used for lava flow simulations characterizing summit eruptions (6 classes in total): 3 classes for short-lived events, lasting from 2 to 10 hours (a) and 3 classes for sub-terminal eruptions, lasting from 4 to 46 days (b).

2.3 Numerical modelling of lava flow paths

We simulated a large number of eruptive scenarios using GPUFLOW (Cappello et al., 2022), a physics-based numerical model for lava flow simulations developed as an improvement of the MAGFLOW model (Cappello et al., 2016). To simulate lava flow paths, GPUFLOW requires constraints of different parameters, including the digital

representation of the topography over which the lava emplaces, the chemical composition of the lava, an estimate of the effusion rate, and the location of the eruptive vent.

For the topography, we used a Digital Surface Model (DSM), obtained from Pléiades imagery acquired on 9 July 2019 for flank eruptions and in July 2021 for summit activity (Ganci et al., 2023). For the chemical composition of the lava, we used a variable viscosity relationship with the typical properties of Etna's basaltic rocks (Giordano and Dingwell, 2003), parameterized in terms of temperature and water content. Typical parameters of Etna's lava, used to run GPUFLOW simulations, are summarized in Table 2.

Input parameter	Value
Extrusion temperature	1360 K
Solidification temperature	1143 K
Density	2600 kg m^{-3}
Water content	0.05 wt%

Table 2. Typical parameters of Etna's lava (from Giordano and Dingwell, 2003; Rogic et al., 2019a; 2019b; 2022).

For flank eruptions, locations of eruptive vents are the nodes of a rectangular regular grid of points with 514890-482490 easting and 4191990-4155990 northing (WGS84 UTM 33N), and spacing of 200 m (see grid in Fig. 1a of Sandri et al., 2024). In this way, we obtained 28,928 potential vents (excluding those falling in the sea), from which we ran 10 GPUFLOW simulations, each one representative of a particular eruptive class (see Section 2.2.1). The effusion rates used for each class are the ones shown in Fig. 3. To summarize, we simulated 289,280 flank lava flow scenarios.

For the summit eruptions, we run the simulations from the 776 nodes of a regular grid with 100 m spacing in both directions overlaid on the summit area, within the Ellittico caldera (see grid in Fig. 5a of Zuccarello et al., 2023). For the vents closer to the summit cones, we ran the GPUFLOW simulations for each of the 6 eruptive classes (see Section 2.2.2), while only the 3 classes linked to the sub-terminal eruptions were considered for the potential vents external to the summit cones. The effusion rates used for each class are the ones shown in Fig. 4. To summarize, we simulated 2,688 summit lava flow scenarios.

2.4 Estimation of the inundation probability

The probability of inundation at each point was computed by combining the spatiotemporal probability of new vent opening, the probability of occurrence for each class of expected eruptions, and the overlapping of the GPUFLOW simulations. The total accumulation probability in the considered Δt interval for each point (x,y) of the domain can be expressed as:

$$P(x, y, \Delta t) = 1 - \prod_{i=1}^{V} \prod_{e=1}^{C_i} (1 - \chi_{ie}(x, y) * p_a(v_i, \Delta t) * p_e) \quad (1)$$

where V is the total number of potential vents, C_i is the number of eruptive classes run from the vent v_i, $\chi_{ie}(x,y)$ is a characteristic function that is equal to 1 if the simulation of class e from the vent v_i inundates the point (x,y) and 0 otherwise, $p_a(v_i,\Delta t)$ is the vent opening probability of v_i in the next Δt years, and p_e is the probability of occurrence of the eruptive class *e*. Therefore, P(x,y,Δt) represents the probability that at least one lava flow in the next Δt years inundates the point (x,y), calculated as the complement of the probability that none of the eruptions reaches that

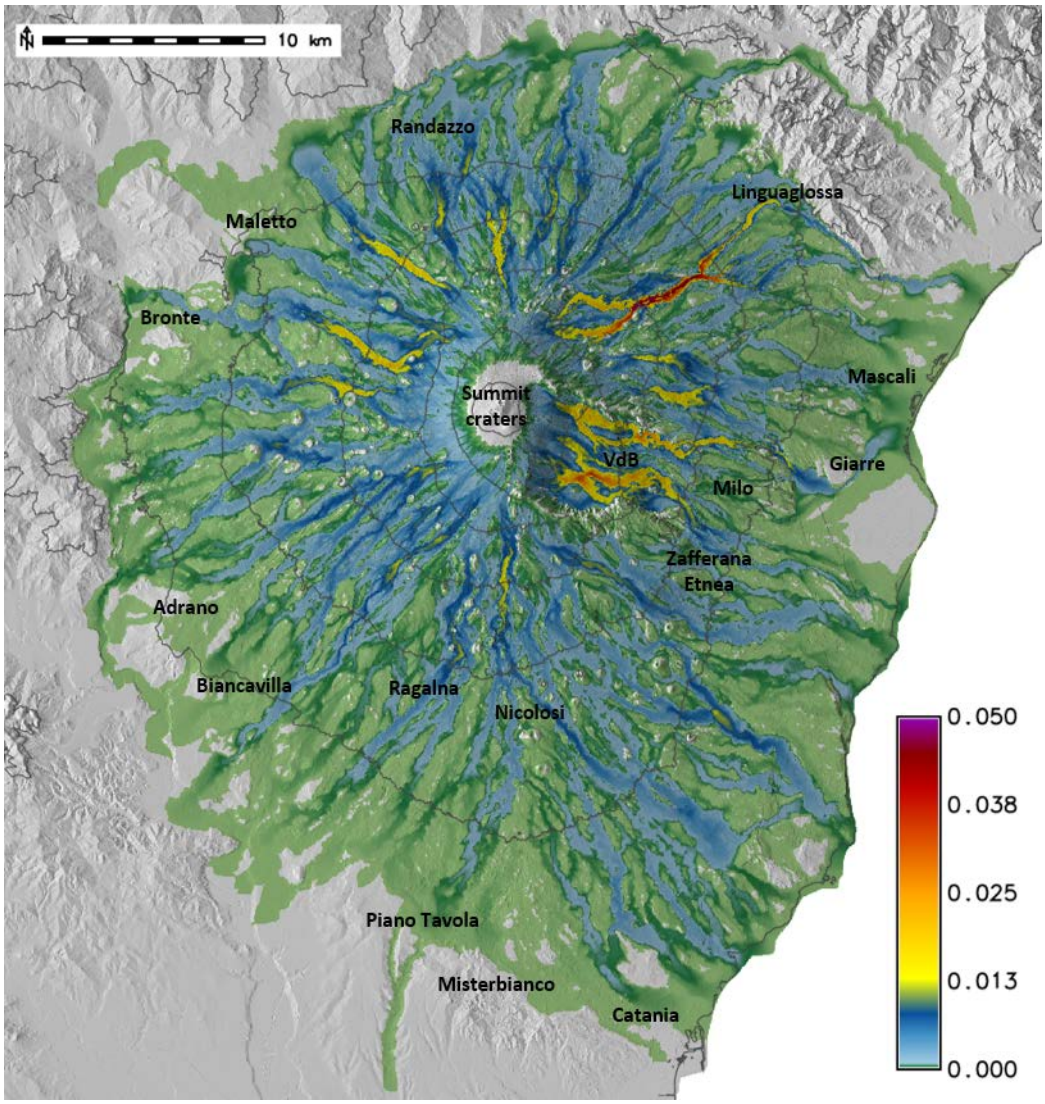

Figure 5. Hazard map by lava flow inundation at Etna volcano based on 289,280 GPUFLOW simulations. Colors represent the different probabilities with which a point can be inundated from a flank lava flow in the next 30 years. Contour lines are from 3,000 to 0 meters a.s.l. (every 500 meters). VdB stands for Valle del Bove.

point. In this estimation, it was assumed that all simulated eruptive scenarios were independent but not mutually exclusive, since all of them can occur without influencing each other (Del Negro et al., 2013b; Bilotta et al., 2023).

The lava flow hazard map for flank eruptions in the next 30 years is reported in Fig. 5. It covers the entire volcanic edifice, reaching altitudes below 500 m a.s.l. in the south flank, skimming the city of Catania and the towns of Misterbianco and Piano Tavola. The highest probabilities (>0.035) are reached inside the Valle del Bove and along the North-East Rift, towards the town of Linguaglossa. Other main population centers exposed to lava inundation, but with lower probabilities (<0.01), include Mascali and Giarre to the east, Milo and Zafferana Etnea to the south-east, Ragalna and Nicolosi to the south, Adrano and Biancavila to the south-west, Bronte and Maletto to the north-west, and Randazzo to the north.

The lava flow hazard map derived from Etna's summit activity in the next 3 years is shown in Fig. 6. The total inundated area is about 41 km^2, reaching the minimum elevation of 1,300 m a.s.l. towards the south-east, inside the Valle del Bove. The highest probabilities (>0.35) are due to lava flows emitted from the SEC, in the northernmost part of the Valle del Bove and in a south-westerly direction, up to an altitude of 2,000 m a.s.l. High probabilities are also reached toward the south-east, again inside Valle del Bove, and to the north-west, up to an elevation of 1,550 m a.s.l. It should be noted that the area potentially affected by summit eruptions has altitudes above 1,500 m a.s.l. (outside Valle del Bove) and does not include inhabited areas.

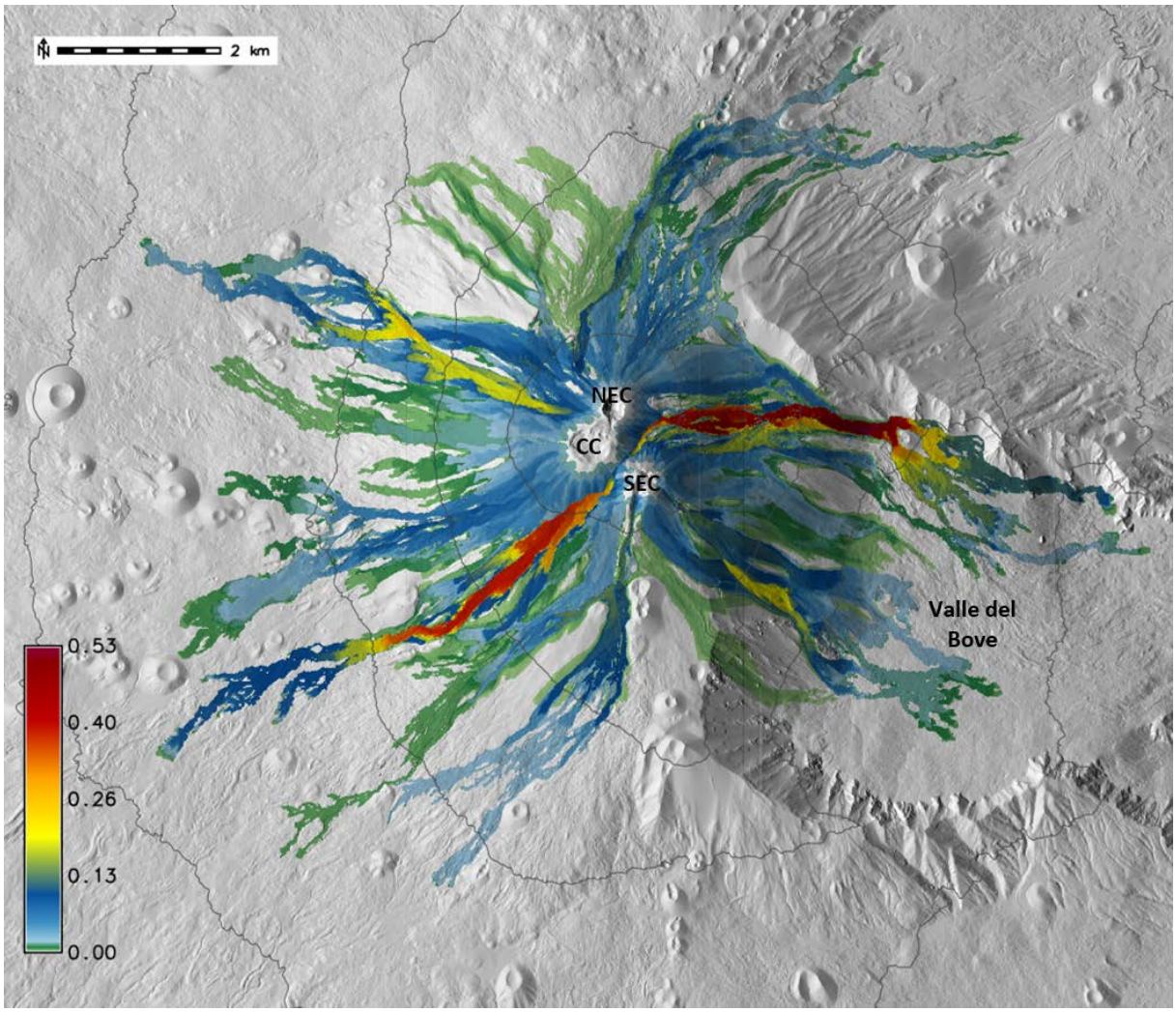

Figure 6. Hazard map by lava flow inundation at Etna volcano based on 2,688 GPUFLOW simulations. Colors represent the different probabilities with which a point can be inundated from a lava flow emitted from a summit eruption in the next 3 years. Contour lines are from 3,000 to 1,500 meters a.s.l. (every 500 meters). CC = Central Crater, NEC = North-East Crater, SEC = South-East Crater (redrawn from Zuccarello et al., 2023).

We also developed the first unified lava flow hazard map that considers lava flows emitted from flank eruptions and summit activity (Fig. 7). First, we developed the probability maps of vent opening considering temporal rates for flank and summit eruptions in the same exposure time of 10 years, chosen as a balance between the different timescales of long-term flank eruptive activity and shorter-term summit activity. Then, we assessed separately the flank and summit hazards. Finally, for each point (x,y) of the domain, we estimated the probability of lava flow inundation once again as the complement of the probability that no flank or summit eruption reaches each point, i.e.:

$$P(x, y, 10) = 1 - \left(1 - P_F(x, y, 10)\right) * \left(1 - P_s(x, y, 10)\right) \quad (2)$$

where $P_F(x,y,10)$ is the hazard from flank eruptions and $P_S(x,y,10)$ is the hazard from summit eruptions in the next 10 years.

The probabilities of this unified map are obviously higher towards the summit area, up to an altitude of 2,000 m a.s.l., while decreasing gradually going down in altitude. The highest probabilities (>0.35) follow the spatial distribution of the summit hazard map (Fig. 6). Obviously the probabilities below 2,000 m are very low (<0.1) both because they are linked to the flank activity which is less frequent than the summit one, and because they are estimated for an exposure time of 10 years, which is very short compared to the long eruptive history of the volcano.

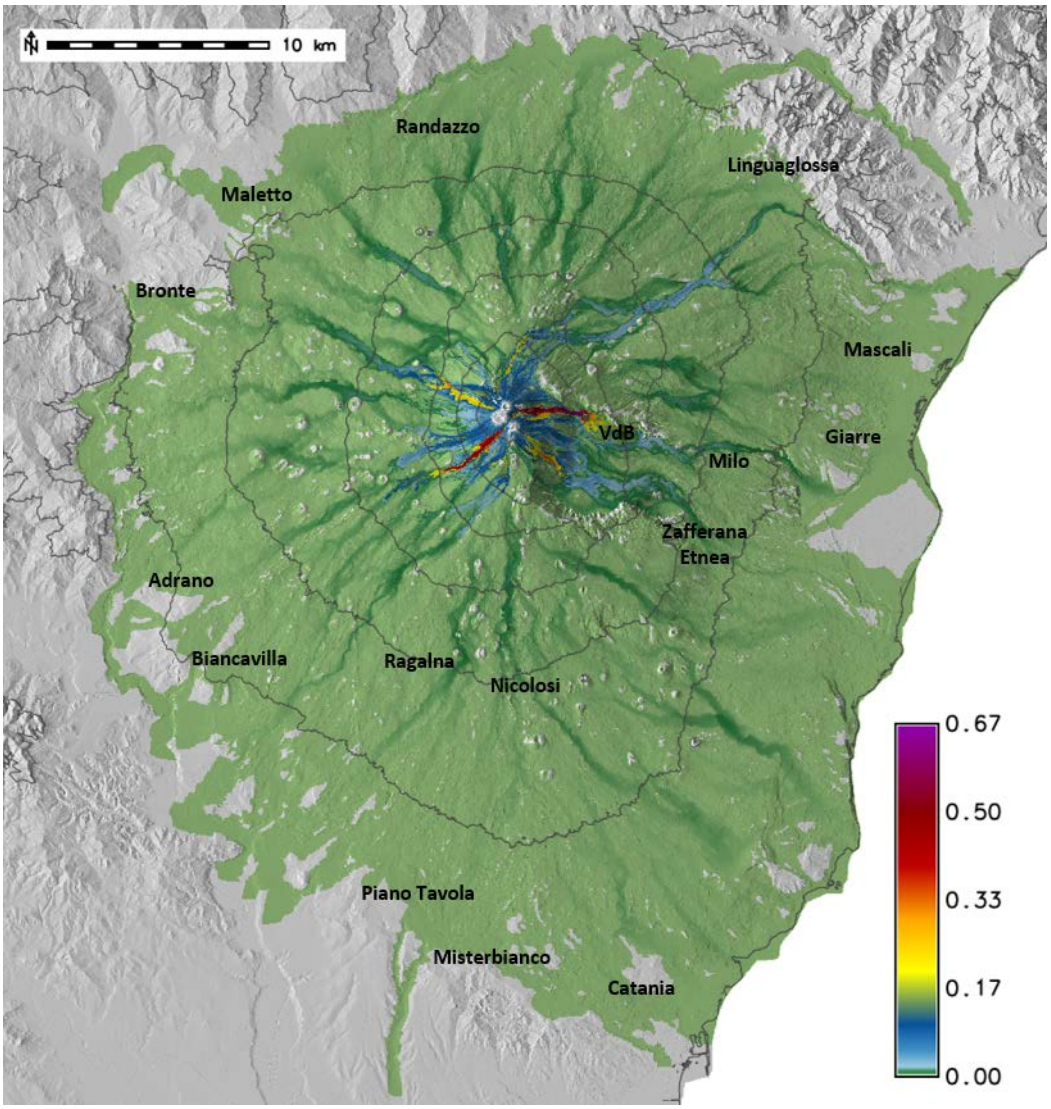

Figure 7. Combined hazard map by lava flow inundation at Etna volcano. Colors represent the different probabilities with which a point can be inundated from a lava flow emitted from a flank or summit eruption in the next 10 years. Contour lines are from 3,000 to 0 meters a.s.l. (every 500 meters).

3. Discussion and Conclusions

Lava flow hazard assessment is important for multiple purposes, including land use planning, promoting safe and sustainable development in volcanic areas, and improving community resilience to volcanic hazards through preparedness and education (Bilotta et al., 2023). This emphasizes the importance of developing up-to-date hazard maps, especially in active volcanoes experiencing concurrent flank and summit eruptive activity, and characterized by several interchanging and growing vents on their summit, such as Etna volcano (Cappello et al., 2019).

In this work, we have provided up-to-date lava flow hazard maps of Etna volcano, obtained through a revised methodology that heavily relies on Etna's eruptive history, starting from the assumption that the locations and characteristics of future eruptions will have the same causal factors as the past ones (Cappello et al., 2013; Sandri et al., 2024).

We have statistically analyzed the historical records of both the flank and summit eruptions of Etna, including the frequency, magnitude, and locations of past lava flows. We have used them to estimate the spatio-temporal probability of future vent opening and to identify styles of expected eruptions, with specific characteristics in duration and total lava volume erupted. These classes of expected eruptions were in turn used to construct characteristic curves of effusive rate (exploiting the statistical analysis of duration and lava volume of historical eruptions) to be used as

input for the GPUFLOW numerical simulations. The probability of future vent opening has been combined with the overlap of the lava flow simulations to obtain three lava flow hazard maps, one for flank eruptions (Fig. 5), one from the summit activity (Fig. 6) and one that considers both (Fig. 7). These three maps highlight the areas more likely to be affected by lava flows over different periods, which mainly depend on the characteristics of the effusive activity.

As expected, the hazard distribution is mainly influenced by the paths and overlap of the lava flow simulations, which strongly depend on the input parameters of the model (especially the water content, the effusion rate and the topography), the sensitivity of which has been analyzed in depth by Bilotta et al. (2012; 2019). However, by comparing our results with the lava flow hazard maps developed in 2013 (Del Negro et al., 2013b), some differences can be immediately noticed. The 2013 lava flow hazard map from flank eruption (*old_flank*) has a sparser spatial distribution than the updated map (*new_flank*), which is instead more homogeneous (Fig. 8). This is undoubtedly due to the spacing of the grid from which the simulations started (at 500 meters in *old_flank vs* 200 meters in *new_flank*), as well as the number of expected eruptive classes (6 in *old_flank vs* 10 in *new_flank*), which increased the number of simulations performed by an order of magnitude (28,908 in *old_flank vs* 289,280 in *new_flank*).

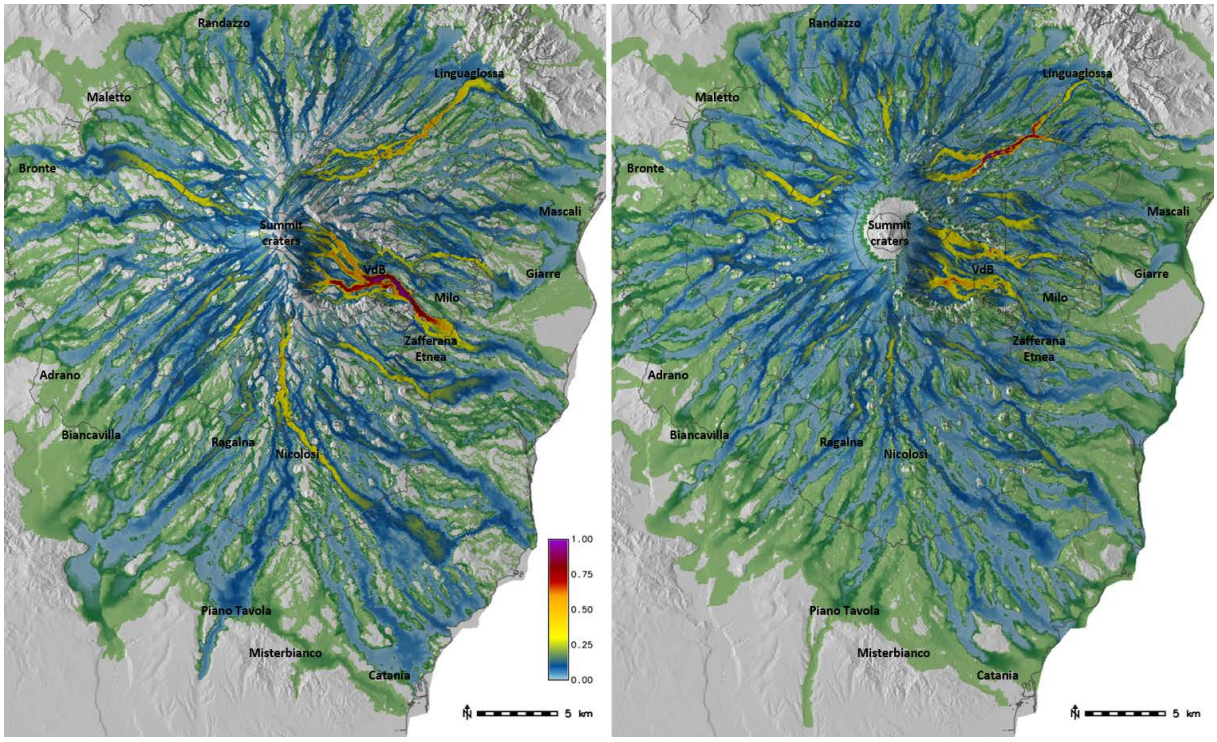

Figure 8. On the left, the lava flow hazard map from flank eruptions updated to 2013 (called *old_flank* in the main text; redrawn from Del Negro et al., 2013b). On the right, the up-to-date hazard map (called *new_flank*). Both maps have been displayed using the same normalized color bar to improve the comparison. Contour lines are from 3,000 to 0 meters a.s.l. (every 500 meters).

In *old_flank*, the highest probabilities are reached inside the Valle del Bove, while in *new_flank*, higher values are reached in the North-East Rift, towards the town of Linguaglossa. This is because the simulations of *old_flank* have been run excluding only the main summit craters, not the whole summit area, which exhibits a particular and different effusive activity from the lateral one. In this way, most of the lava flows emitted from vents in the south-east flank of the volcano, even at very high altitudes (more than 2,800 m a.s.l.) follow the same paths, reaching the Valle del Bove area. The same consideration can be made for the other flanks, even if it is not so evident due to the lack of such a large depression, like the Valle del Bove.

By comparing the 2013 lava flow hazard map from summit eruptions (*old_summit*) with the updated map (*new_summit*), the differences are very evident (Fig. 9). The first and perhaps most important aspect is the extension. Indeed, the inundated area in *old_summit* measures about 51 km^2, while it is 41 km^2 in *new_summit*. Moreover, the

maximum distance of the simulated lava flow paths in *old_summit* reaches about 700 m a.s.l. in the south-east flank, while the longest lava flow paths in *new_summit* reach the minimum elevation of 1,300 m a.s.l. inside the Valle del Bove.

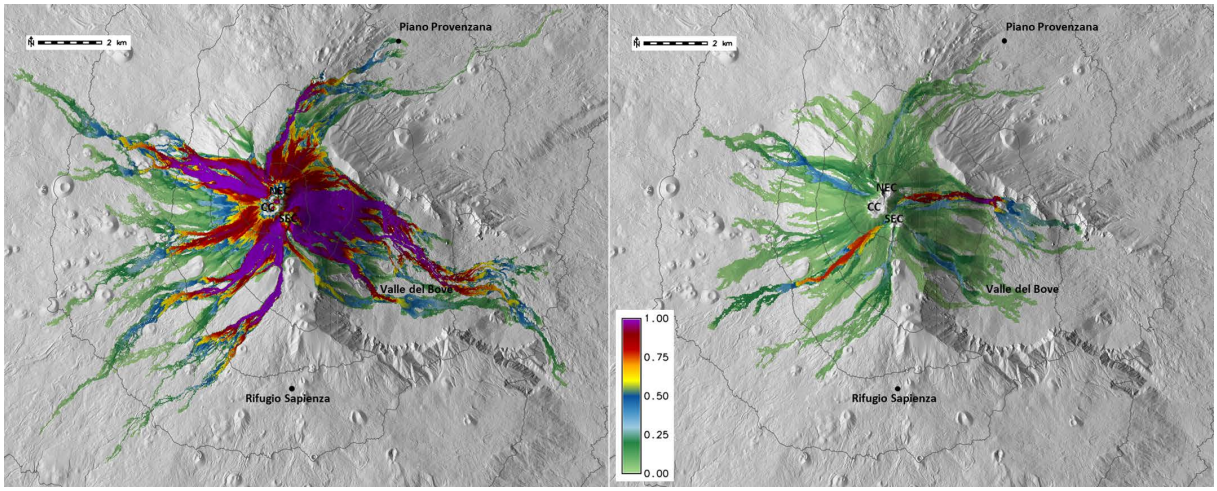

Figure 9. On the left, the lava flow hazard map from summit activity updated to 2013 (called *old_summit* in the main text; redrawn from Del Negro et al., 2013b). On the right, the up-to-date hazard map (called *new_summit*; redrawn from Zuccarello et al., 2023). Both maps have been displayed using the same normalized color bar to improve the comparison. Contour lines are from 3,000 to 1,000 meters a.s.l. (every 500 meters).

The areas with the highest probability of inundation in *old_summit* are very large, making the preferential paths of the lava unclear. Conversely, *new_summit* highlights that, with the current morphology of the terrain, the more likely areas to be inundated by future lava flows are the northernmost part of the Valle del Bove, in the south-westerly direction, and toward north-west. Finally, in *old_summit*, the northern tourist facility of Piano Provenzana is exposed to lava inundation, while it is not covered in *new_summit*. The southern tourist facility of Rifugio Sapienza is shielded from the pyroclastic cones formed during the flank eruptions in 2001 and 2002-2003, which naturally divert the lava west or east of the cones.

These differences highlight the need to develop innovative methodologies for the estimate of the hazard, providing increasingly accurate and reliable maps, which can be used both for the management of emergencies, and for territorial planning.

Data availability statement. Figures were generated using the free and open source GRASS GIS software. The Geotiff maps of the flank and summit lava flow hazard can be downloaded from the Open Data portal of the INGV-Osservatorio Etneo, respectively, at the links https://doi.org/10.13127/volc_hazard/etna_flank_lava_2023 and https://doi.org/10.13127/volc_hazard/etna_summit_lava_2023.

Acknowledgements. This work was supported by the INGV project Pianeta Dinamico (CUP D53J19000170001) funded by MIUR ("Fondo finalizzato al rilancio degli investimenti delle amministrazioni centrali dello Stato e allo sviluppo del Paese", Legge 145/2018), Tema 8 – PANACEA 2021-2023.

References

Behncke B., M. Neri and A. Nagay (2005). Lava flow hazard at Mount Etna (Italy): new data from a GIS-based study. M. Manga, G. Ventura (Eds.), Kinematics and Dynamics of Lava Flows, Geological Society of America Special Paper, 396, 189-208, doi:10.1130/0-8137-2396-5.189.

Bevilacqua, A., M. Bursik, A., Patra, E. Pitman, et al. (2017). Bayesian construction of a long-term vent opening probability map in the Long Valley volcanic region (CA, USA), Statist. Volcanol., 3, 1, doi:10.5038/2163-338X.3.1.

Bilotta, G., A. Cappello, A. Hérault, A. Vicari et al. (2012). Sensitivity analysis of the MAGFLOW Cellular Automaton model for lava flow simulation. Environ. Model. Softw., 35, 122-131, doi:10.1016/j.envsoft.2012.02.015.

Bilotta, G., A. Cappello, A. Hérault, C. Del Negro (2019). Influence of topographic data uncertainties and model resolution on the numerical simulation of lava flows, Environ. Model. Softw. 112, 1-15, doi:10.1016/j.envsoft.2018.11.001.

Bilotta, G., A. Cappello and G. Ganci (2023). Formal Matters on the Topic of Risk Mitigation: A Mathematical Perspective, Appl. Sci., 13, 265, doi:10.3390/app13010265.

Branca, S. and P. Del Carlo (2005). Types of eruptions of Etna volcano AD 1670-2003: Implications for short-term eruptive behaviour, Bull. Volcanol., 67, 732-742, doi:10.1007/s00445-005-0412-z.

Branca, S., M. Coltelli, G. Groppelli and F. Lentini (2011). Geological map of Etna volcano, 1:50,000 scale, Ital. J. Geosci., 130 3, 265-291, doi:10.3301/IJG.2011.15.

Branca, S., E. De Beni and C. Proietti (2013). The large and destructive 1669 AD eruption at Etna volcano: reconstruction of the lava flow field evolution and effusion rate trend, Bull Volcanol., 75, 694, doi:10.1007/s00445-013-0694-5.

Branca, S., E. De Beni, D. Chester, A. Duncan et al. (2017). The 1928 eruption of Mount Etna (Italy): Reconstructing lava flow evolution and the destruction and recovery of the town of Mascali, J. Volcanol. Geotherm. Res., 335, 54-70, doi:10.1016/j.jvolgeores.2017.02.002.

Cappello, A., A. Vicari and C. Del Negro (2011a). Assessment and modeling of lava flow hazard on Etna volcano, Boll. Geof. Teor. Appl., 52, 299-308, doi:10.4430/bgta0003.

Cappello, A., A. Vicari and C. Del Negro (2011b). Retrospective validation of a lava-flow hazard map for Mount Etna volcano, Ann. Geophys., 54, 634-640, doi:10.4401/ag-5345.

Cappello, A., G. Bilotta, M. Neri and C. Del Negro (2013). Probabilistic modeling of future volcanic eruptions at Mount Etna, J. Geophys. Res., 118, 1925-1935, doi:10.1002/jgrb.50190.

Cappello, A., N. Geshi, M. Neri and C. Del Negro (2015). Lava flow hazards-An impending threat at Miyakejima volcano, Japan, J. Volcanol. Geotherm. Res., 308, 1-9, doi:10.1016/j.jvolgeores.2015.10.005.

Cappello, A., G. Ganci, G. Bilotta, C. Corradino et al. (2019). Changing Eruptive Styles at the South-East Crater of Mount Etna: Implications for Assessing Lava Flow Hazards, Front. Earth Sci., 7, 213, doi:10.3389/feart.2019.00213.

Cappello, A., G. Bilotta and G. Ganci (2022). Modeling of geophysical flows through GPUFLOW, Appl. Sci., 12, 4395, doi:10.3390/app12094395.

Centorrino, V., G. Bilotta, A. Cappello, G. Ganci et al. (2021). A particle swarm optimization-based heuristic to optimize the configuration of artificial barriers for the mitigation of lava flow risk, Environ. Model. Softw., 2021, 139, 105023.

Cioni, R., D. Andronico, L. Cappelli, A. Aravena et al. (2023). Products and dynamics of lava-snow explosions: The 16 March 2017 explosion at Mount Etna, Italy, GSA Bulletin, 136, 5-6, 2325-2342, doi:10.1130/B37102.1.

Coltelli, M., M. Marsella, C. Proietti and S. Scifoni (2012). The case of the 1981 eruption of Mount Etna: An example of very fast moving lava flows, Geochem. Geophys. Geosyst., 13, Q01004, doi:10.1029/2011GC003876.

Crisci, G. M., M. V. Avolio, B. Behncke, D. D'Ambrosio et al. (2010). Predicting the impact of lava flows at Mount Etna, Italy, J. Geophys. Res., 115, B04203, doi:10.1029/2009JB006431.

Del Negro, C, A. Cappello, M. Neri, G. Bilotta et al. (2013a). Etna flank lava flows between 1610 and 2008 [dataset], PANGAEA, doi:10.1594/PANGAEA.825012.

Del Negro, C., A. Cappello, M. Neri, G. Bilotta et al. (2013b). Lava flow hazards at Mount Etna: constraints imposed by eruptive history and numerical simulations, Sci. Rep., 3, 3493, doi:10.1038/srep03493.

Del Negro, C., A. Cappello, G. Bilotta, G. Ganci et al. (2020). Living at the edge of an active volcano: Risk from lava flows on Mt. Etna, GSA Bull., 132, 7-8, 1615-1625, doi:10.1130/B35290.1.

Duncan, A. M., D. K. Chester and J. E. Guest (1981). Mount Etna Volcano: environmental impact and problems of volcanic prediction, Geogr. J., 147, 164-179, doi:10.2307/634532.

Favalli, M., S. Tarquini, A. Fornacia and E. Boschi (2009). A new approach to risk assessment of lava flow at Mount Etna, Geology, 37, 12, 1111-1114, doi:10.1130/G30187A.1.

Frazzetta, G. and R. Romano (1978). Approccio de studio per la stesura di una carta del rischio vulcanico (Etna, Sicilia), Mem. Soc. Geol. Ital., 19, 691-697.

Ganci, G., A. Cappello and M. Neri (2023). Data Fusion for Satellite-Derived Earth Surface: The 2021 Topographic Map of Etna Volcano, Remote Sens., 15, 198, doi:10.3390/rs15010198.

Garcia-Aristizabal, A., W. Marzocchi and E. Fujita (2012). A Brownian model for recurrent volcanic eruptions: an application to Miyakejima volcano (Japan), Bull. Volcanol., 74, 545-558, doi:10.1007/s00445-011-0542-4.

Giordano, D. and D. B. Dingwell (2003). Viscosity of hydrous Etna basalt: implications for Plinian-style basaltic eruptions, Bull. Volcanol., 65, 8-14, doi:10.1007/s00445-002-0233-2.

Guest, J. E. and J. B. Murray (1979). An analysis of hazard from Mount Etna Volcano, J. Geol. Soc. London, 136, 347-354, doi:10.1144/gsjgs.136.3.0347.

Gwinner, K., M. Coltelli, J. Flohrera, R. Jaumanna et al. (2006). The HRSC-AX Mt. Etna Project: High-resolution Orthoimages and 1 m DEM at Regional Scale, In Proceedings of the ISPRS XXXVI, Paris, France, 4-6 July 2006, T05-23.

Mangiameli, M., A. Cappello and G. Mussumeci (2025). Spatial data and GIS for the assessment of the environmental impact at Mount Etna, Ann. Geophys., 68, doi:10.4401/ag-9171.

Proietti, C. and S. Branca (2024). Dataset of Etna's flank eruptive fissures of the last 4000 years [Data set], Zenodo, doi:10.5281/zenodo.14284932.

Rogic, N., A. Cappello and F. Ferrucci (2019a). Role of Emissivity in Lava Flow 'Distance-to-Run' Estimates from Satellite-Based Volcano Monitoring, Remote Sens., 11, 662, doi:10.3390/rs11060662.

Rogic, N., A. Cappello, G. Ganci, A. Maturilli et al. (2019b). Spaceborne EO and a combination of inverse and forward modelling for monitoring lava flow advance, Remote Sens., 11, 3032, doi:10.3390/rs11243032.

Rogic, N., G. Bilotta, G. Ganci and J. O. Thompson et al. (2022). The Impact of Dynamic Emissivity-Temperature Trends on Spaceborne Data: Applications to the 2001 Mount Etna Eruption, Remote Sens., 14, 1641, doi:10.3390/rs14071641.

Sandri, L., A. Garcia, C. Proietti, S. Branca et al. (2024). Where will the next flank eruption at Etna occur? An updated spatial probabilistic assessment, Nat. Hazards Earth Syst. Sci., 24, 4431-4455, doi:10.5194/nhess-24-4431-2024.

Selva, J., G. Orsi, M. Di Vito, W. Marzocchi et al. (2012). Probability hazard map for future vent opening at the Campi Flegrei caldera, Italy, Bull. Volcanol., 74, 2, 497-510, doi:10.1007/s00445-011-0528-2.

Smethurst, L., M. R. James, H. Pinkerton and J. A. Tawn (2009). A statistical analysis of eruptive activity on Mount Etna, Sicily, Geophys. J. Int., 179, 655-666, doi:10.1111/j.1365-246X.2009.04286.x.

Vicari, A., G. Ganci, B. Behncke, A. Cappello et al. (2011). Near-real-time forecasting of lava flow hazards during the 12-13 January 2011 Etna eruption, Geophys. Res. Lett., 38, L13317, doi:10.1029/2011GL047545.

Wadge, G., P. A. V. Young and I. J. McKendrick (1994). Mapping lava flow hazards using computer simulation, J. Geophys. Res., 99, B1, 489-504, doi:10.1029/93JB01561.

Zuccarello, F., G. Bilotta, A. Cappello and G. Ganci (2022). Effusion Rates on Mt. Etna and Their Influence on Lava Flow Hazard Assessment, Remote Sens., 14, 1366, doi:10.3390/rs14061366.

Zuccarello, F., G. Bilotta, G. Ganci and C. Proietti et al. (2023). Assessing impending hazards from summit eruptions: the new probabilistic map for lava flow inundation at Mt. Etna, Sci Rep., 13, 19543, doi:10.1038/s41598-023-46495-0.

***CORRESPONDING AUTHOR: Annalisa CAPPELLO**,
Istituto Nazionale di Geofisica e Vulcanologia, Osservatorio Etneo, Catania, Italy
e-mail: annalisa.cappello@ingv.It